



Eigenmodes in a \mathcal{PT} -symmetric waveguide: Complex dispersion curves

Nan Zhang * and Ya Yan Lu 

Department of Mathematics, City University of Hong Kong, Kowloon, Hong Kong, China



(Received 28 December 2023; accepted 30 April 2024; published 10 May 2024)

Many novel wave phenomena have been observed in parity-time (\mathcal{PT})-symmetric optical waveguides with a balanced gain and loss. These phenomena are highly related to the eigenmodes which are solutions of Maxwell's equation without sources. An eigenmode is associated with a propagation constant and an angular frequency. Most existing studies are concerned with guided modes at a real frequency. In this paper, we analyze various eigenmodes in a \mathcal{PT} -symmetric slab waveguide, including guided modes with a complex frequency or a complex propagation constant, leaky modes, resonant modes, lasing-threshold modes, and perfect-absorption modes. We study the dispersion curves of eigenmodes and focus on the connection between the real and complex eigenmodes. It is observed that as the amplitude of balanced gain and loss is varied, there exist a few transition points where the connections between real and complex eigenmodes exhibit abrupt changes. In particular, there exists a transition point corresponding to the emergence of lasing-threshold and perfect-absorption modes. It is expected that the wave phenomena revealed in this paper are generic and can be found in other \mathcal{PT} -symmetric waveguides. Our work improves theoretical understanding on \mathcal{PT} -symmetric waveguides, and may have potential applications in non-Hermitian photonics.

DOI: [10.1103/PhysRevA.109.053515](https://doi.org/10.1103/PhysRevA.109.053515)

I. INTRODUCTION

In recent years, optical structures with parity-time (\mathcal{PT}) symmetry have attracted extensive research in the photonics community [1–15]. Many interesting wave phenomena, including unidirectional reflectionless propagation [16–19], Bloch oscillations [20], single-mode lasing [21,22], and simultaneous lasing and coherent perfect absorption [23–25], have been observed in \mathcal{PT} -symmetric systems. A widely studied \mathcal{PT} -symmetric structure is an optical waveguide with a balanced gain and loss [4–6,8,10,26–38]. The dielectric function of such a waveguide has a symmetric real part and an antisymmetric imaginary part with respect to a spatial variable perpendicular to the waveguide axis. Many studies on \mathcal{PT} -symmetric waveguides are concerned with guided modes at a fixed real angular frequency ω for a varying amplitude σ of the balanced gain and loss [4,26–32]. There are also some works focusing on the dispersion curves of guided modes [33–38]. In our recent work [38], we analyzed the dependence on σ for the dispersion curves of guided modes with a real ω and a real propagation constant β .

In many existing works on \mathcal{PT} -symmetric optical waveguides, it has been shown that for a given ω , two or more real guided modes merge to a single mode as σ is increased to a critical value [the exceptional point (EP)], and guided modes with a complex β emerge for σ larger than the critical value [4,26–32]. In fact, EPs can also be formed for a fixed σ , when ω or β are considered as the parameter, and guided modes with a complex β or ω emerge when the parameter passes through the critical value [35–38].

Guided modes are proper modes that decay to zero in the lateral direction. It is also useful to study improper modes that do not decay as the lateral variable tends to infinity [39–46]. A leaky mode is an improper mode satisfying an outgoing radiation condition [39–42]. It has a real ω and a complex β , decays in the forward propagation direction, and diverges in the lateral direction. In connection with scattering problems where incident waves are specified in the cladding or the substrate of the waveguide, it is useful to consider resonant modes. A resonant mode is also an improper mode satisfying an outgoing radiation condition [43–46]. It has a real β and a complex ω , decays with time t , and diverges in the lateral direction. In slab waveguides, there exist real improper modes which have a real β , a real ω , and a divergent field. It is known that the complex dispersion curves of leaky and resonant modes are connected with the dispersion curves of real improper modes [45,46].

In addition to the guided modes and the improper modes mentioned above, a \mathcal{PT} -symmetric waveguide may have lasing-threshold modes and perfect-absorption modes with the same frequency ω and the same propagation constant β [23–25,44]. A lasing-threshold mode radiates power laterally and a perfect-absorption mode absorbs power coming from infinity. They are also improper eigenmodes since their fields do not decay in the lateral direction (remain bounded at infinity).

For \mathcal{PT} -symmetric waveguides, it is important to investigate the eigenmodes since they are essential to many novel wave phenomena. In this paper, we study guided modes with a complex β or ω and various improper modes. We focus on the connection between the dispersion curves of different eigenmodes, analyze the dependence of dispersion curves on σ , and show that there exist interesting transition points as σ is varied. A particular interesting transition point corresponds

*nzhang234-c@my.cityu.edu.hk

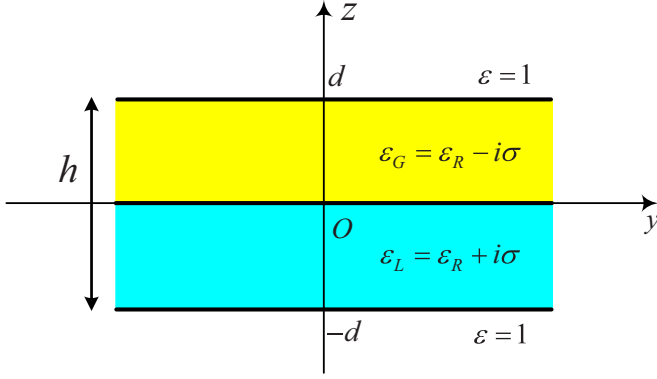


FIG. 1. A \mathcal{PT} -symmetric slab waveguide with thickness $h = 2d$ and surrounded by air.

to the emergence of lasing-threshold and perfect-absorption modes. For simplicity, we follow Ref. [4] and consider a \mathcal{PT} -symmetric slab waveguide. However, we believe the wave phenomena revealed in this paper also exist in other \mathcal{PT} -symmetric waveguides.

The rest of this paper is organized as follows. In Sec. II, we recall the definition of various eigenmodes in \mathcal{PT} -symmetric waveguides. In Sec. III, we analyze the dependence on σ for the dispersion curves of real improper modes. In Sec. IV, we study the connection between the complex dispersion curves and the dispersion curves of real guided and real improper modes. The paper is concluded by a summary in Sec. V.

II. EIGENMODES IN A \mathcal{PT} -SYMMETRIC SLAB WAVEGUIDE

We consider a \mathcal{PT} -symmetric slab waveguide surrounded by air as shown in Fig. 1. A Cartesian coordinate system is chosen so that the dielectric function ε depends only on z . The thickness of the slab is $h = 2d$, and for $|z| > d$, we have $\varepsilon = 1$. The dielectric constants of the upper ($0 < z < d$) and lower ($-d < z < 0$) parts of the slab are $\varepsilon_G = \varepsilon_R - i\sigma$ and $\varepsilon_L = \varepsilon_R + i\sigma$, respectively, where ε_R and σ are constants, $\varepsilon_R > 1$, and $\sigma \geq 0$ is the amplitude of the balanced gain and loss. Thus the dielectric function ε is \mathcal{PT} symmetric, i.e., it satisfies $\varepsilon(z) = \bar{\varepsilon}(-z)$, where $\bar{\varepsilon}$ is the complex conjugate of ε . Notice that if $\sigma = 0$, the waveguide is a lossless symmetric slab waveguide.

Assuming the field is invariant in x , the electric field of a transverse electric (TE) eigenmode only has a nonzero x component E_x given by

$$E_x = \text{Re}[u(z)e^{i(\beta y - \omega t)}], \quad (1)$$

where $u(z)$ is the mode profile, β is the propagation constant, and ω is the angular frequency. The mode profile u satisfies the following one-dimensional (1D) Helmholtz equation,

$$\frac{d^2 u}{dz^2} + k_0^2 \varepsilon(z) u = \beta^2 u, \quad -\infty < z < \infty, \quad (2)$$

where $k_0 = \omega/c$ is the free-space wave number and c is the speed of the light in vacuum. Since ε_R and σ are constants, it

can be shown that k_0 and β satisfy the dispersion equation

$$\mathcal{H}(k_0, \beta) = 0, \quad (3)$$

where $\mathcal{H} = \mathcal{H}_1(k_0, \beta) + \mathcal{H}_2(k_0, \beta)$,

$$\mathcal{H}_1 = \kappa(\gamma \cos \kappa - i\kappa \sin \kappa)(\gamma \sin \bar{\kappa} + i\bar{\kappa} \cos \bar{\kappa}),$$

$$\mathcal{H}_2 = \bar{\kappa}(\gamma \sin \kappa + i\kappa \cos \kappa)(\gamma \cos \bar{\kappa} - i\bar{\kappa} \sin \bar{\kappa}),$$

$\gamma = d\sqrt{k_0^2 - \beta^2}$, and $\kappa = d\sqrt{k_0^2 \varepsilon_G - \beta^2}$. In this paper, we consider eigenmodes with real or complex β and k_0 .

Guided modes satisfy $u \rightarrow 0$ as $z \rightarrow \pm\infty$. A real guided mode (RGM) has a real k_0 and a real β . If $u(z)$ is the profile of an RGM, then $\bar{u}(-z)$ is also a mode profile for the same RGM. Therefore, we can build a new profile $\hat{u}(z) := u(z) + \bar{u}(-z)$ which is \mathcal{PT} symmetric, i.e., $\hat{u}(z) = \hat{u}(-z)$. If the mode is nondegenerate, there exists a constant C such that $\hat{u} = Cu$. RGMs can form curves in the β - k_0 plane, and these dispersion curves are connected to the lightlines, $k_0 = \pm\beta$, at the cutoff points with a cutoff wave number k_c .

In \mathcal{PT} -symmetric waveguides, a guided mode can also have a complex β and a real k_0 . Its amplitude decreases or increases along the forward propagation direction. We call such a mode a complex-propagation-constant guided mode (CPGM). In this case, the \mathcal{PT} symmetry of the system is broken. The mode profile u of a CPGM also cannot be scaled to satisfy \mathcal{PT} symmetry. It can be shown that $\bar{u}(-z)$ is the mode profile of a CPGM with the propagation constant $\bar{\beta}$ and the same k_0 . As shown in Ref. [38], there also exist guided modes with a complex k_0 and a real β . We call such a mode a complex-frequency guided mode (CFGM). A CFGM with $\text{Im}(k_0) < 0$ decays exponentially with time t . The mode profile u cannot be scaled to satisfy \mathcal{PT} symmetry and $\bar{u}(-z)$ is the mode profile of a CFGM with the wave number \bar{k}_0 and the same β .

Guided modes are proper modes which decay to zero in the lateral direction. In \mathcal{PT} -symmetric slab waveguides, there also exist improper modes which do not decay to zero laterally. A real improper mode (RIM) has a real k_0 and a real β , and diverges in the lateral direction. RIMs exist below the lightline and form curves connected to the lightlines at the cutoff points. A leaky mode has a real k_0 and a complex β , decays in the forward propagation direction, and diverges in the lateral direction. It is an improper mode satisfying an outgoing radiation condition, i.e., it radiates out power in the lateral direction to infinity ($z \rightarrow \pm\infty$). For a leaky mode with a profile $u(z)$, we can obtain another eigenmode with the same k_0 , the propagation constant $\bar{\beta}$, and the profile $\bar{u}(-z)$. Such a mode also diverges in the lateral direction but satisfies an incoming-wave condition, i.e., it absorbs power laterally from infinity. Its amplitude increases along the forward propagation direction since the power coming from infinity concentrates on the slab. This mode can be interpreted as the time reversal of a leaky mode.

A resonant mode has a real β and a complex k_0 with $\text{Im}(k_0) < 0$. It decays exponentially with time t , diverges in the lateral direction, and satisfies an outgoing radiation condition. For a resonant mode with a profile $u(z)$, we can obtain its time reversal which has the same β , the free-space wave number \bar{k}_0 and the profile $\bar{u}(-z)$. The time-reversed resonant

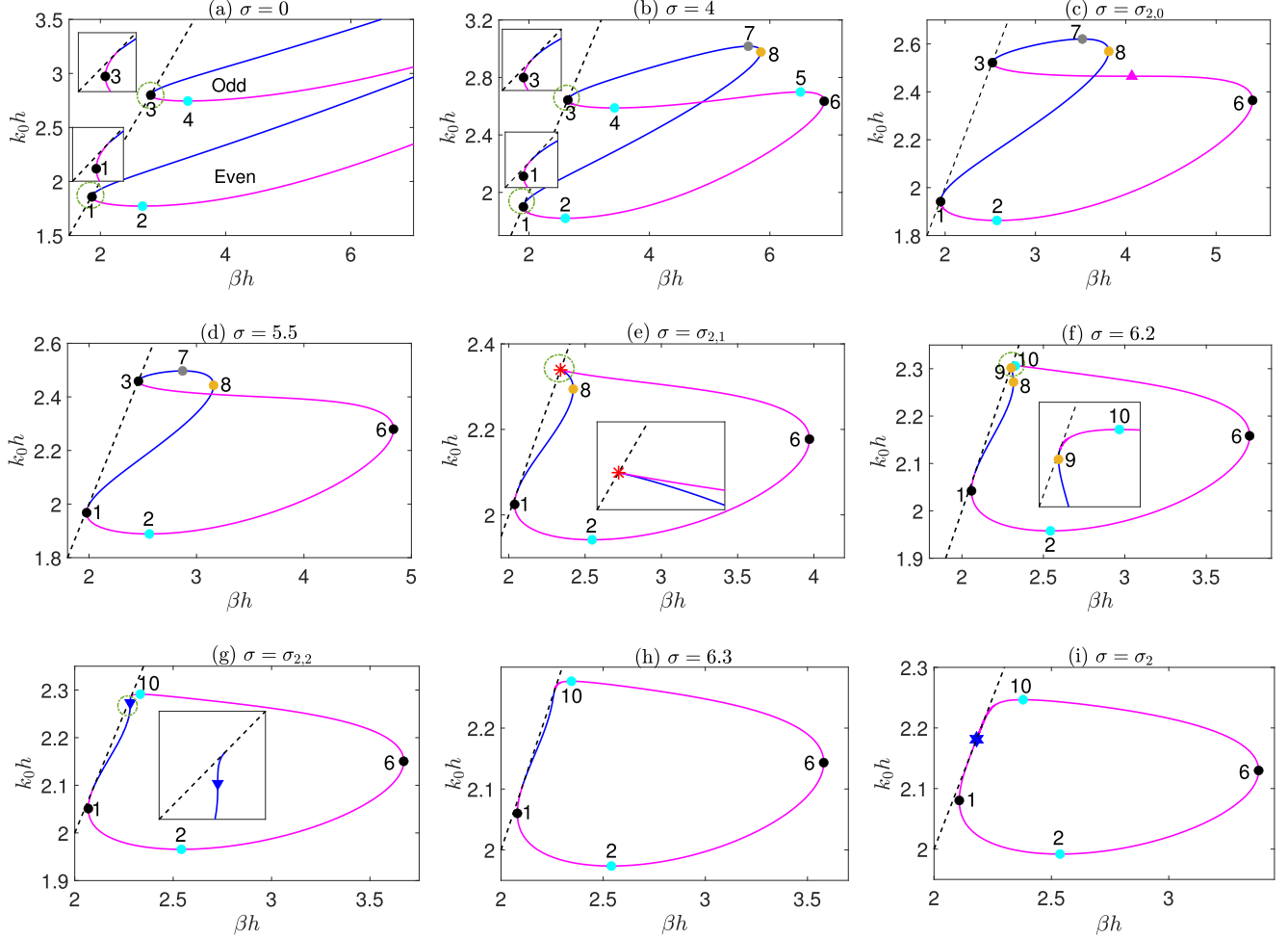


FIG. 2. The dispersion curves of RGMs (blue) and RIMs (magenta) of a \mathcal{PT} -symmetric slab waveguide for an increasing sequence of σ . The dashed black lines represent the lightline. The dots and triangles represent second-order and third-order EPs, respectively. The red asterisk represents the cutoff point with $k_c h \approx 2.3392$, where the second dispersion curve of RGMs is not tangential to the lightline. At $\sigma = \sigma_2$, the dispersion curve of RGMs degenerates to a single point marked by a blue hexagram on the lightline.

mode satisfies an incoming-wave condition and also diverges in the lateral direction.

Leaky and resonant modes have been widely studied in open dielectric waveguides. In \mathcal{PT} -symmetric waveguides, there exist some special improper modes that do not exist in lossless waveguides. A lasing-threshold mode has a real β and a real k_0 satisfying $k_0 > |\beta|$. It satisfies an outgoing radiation condition [44] and remains bounded in the infinity. The mode profile u cannot be scaled to satisfy \mathcal{PT} symmetry and $\bar{u}(-z)$ is the mode profile of another eigenmode with the same k_0 and the same β . Such a mode is called a perfect-absorption mode and satisfies an incoming-wave condition [44].

III. DEPENDENCE ON σ FOR THE DISPERSION CURVES OF REAL IMPROPER MODES

In a recent work [38], we analyzed the dependence of dispersion curves of RGMs on σ . It was shown that there exist a finite number of dispersion curves for any positive σ . Each dispersion curve is connected to the lightline at two cutoff points. The l th dispersion curve of RGMs can only exist for $\sigma < \sigma_l$, and when $\sigma = \sigma_l$, it degenerates to a single point

on the lightline. Moreover, the dispersion curve exhibits two interesting transition points $\sigma_{l,1}$ and $\sigma_{l,2}$ satisfying $0 < \sigma_{l,1} < \sigma_{l,2} < \sigma_l$.

It is also useful to study the dispersion curves of RIMs since they are connected with leaky and resonant modes [45,46]. Without loss of generality, we consider a \mathcal{PT} -symmetric slab waveguide with $\varepsilon_R = 12.25$ and study the second dispersion curves for RGMs and RIMs. The case for $l \neq 2$ is similar. In Fig. 2, we show the dispersion curves for $\sigma = 0, 4, \sigma_{2,0}, 5.5, \sigma_{2,1}, 6.2, \sigma_{2,2}, 6.3, \sigma_2$, where $\sigma_{2,1} \approx 6.0803$, $\sigma_{2,2} \approx 6.2517$, $\sigma_2 \approx 6.3952$, and $\sigma_{2,0} \approx 5.0803$ is a transition point for the dispersion curve of RIMs. As $\sigma \rightarrow 0$, the second dispersion curves approach the second even and odd dispersion curves of RGMs and RIMs of a lossless symmetric slab waveguide, as shown in Fig. 2(a). It is observed that for a positive $\sigma < \sigma_2$, the dispersion curves of RIMs and RGMs are connected at two cutoff points on the lightline. The dispersion curves contain local extremum points which are marked by dots and associated integers. When σ passes through a transition point, the extremum points may disappear or emerge.

In fact, these local extremum points on the dispersion curves are EPs. For a non-Hermitian eigenvalue problem with

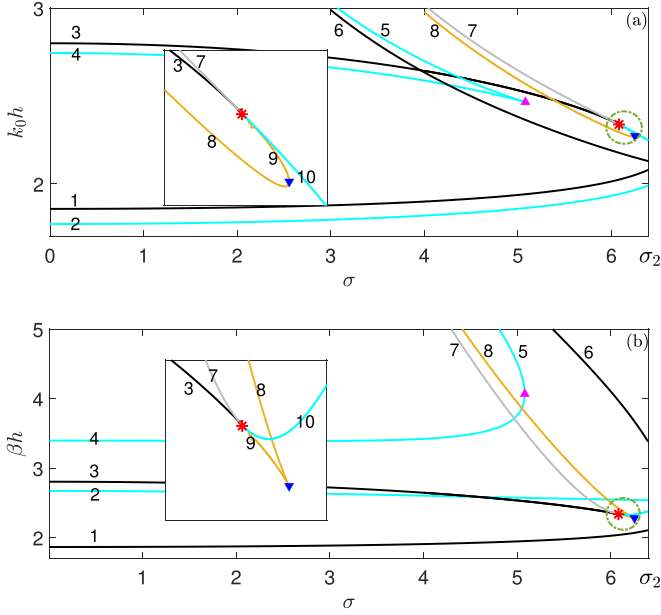


FIG. 3. The free-space wave number k_0 and the propagation constant β of EPs vs σ . The magenta upward and blue downward triangles correspond to $\sigma_{2,0}$ and $\sigma_{2,2}$, respectively. The red asterisk corresponds to $\sigma_{2,1}$. As σ is increased to $\sigma_{2,1}$, EPs 3 and 7 coalesce at the cutoff point with $k_c h \approx 2.3392$.

some parameters, an EP of order N is the critical values of the parameters, such that when the parameters tend to the critical values, N eigenvalues and their corresponding eigenfunctions merge to a single eigenvalue and a single eigenfunction, respectively. For a fixed σ , Eq. (2) can be regarded as an eigenvalue problem with a parameter β or k_0 . The eigenfunction is the mode profile $u(z)$. If β is regarded as the parameter, then k_0^2 or k_0 is the eigenvalue. As β approaches a local extremum ($d\beta/dk_0 = 0$), two or more different eigenvalues k_0 and their corresponding eigenfunctions merge to a single eigenvalue and a single eigenfunction, respectively. We call a local extremum point in β a β -EP. It can be solved from

$$\mathcal{H}(k_0, \beta) = 0, \quad \frac{\partial \mathcal{H}}{\partial k_0} = 0. \quad (4)$$

Similarly, if k_0 is regarded as the parameter, then β^2 or β is the eigenvalue. We call a local extremum point in k_0 ($dk_0/d\beta = 0$) a k_0 -EP, and it can be solved from

$$\mathcal{H}(k_0, \beta) = 0, \quad \frac{\partial \mathcal{H}}{\partial \beta} = 0. \quad (5)$$

Figure 2 illustrates the evolution of the second dispersion curves as σ is increased from zero to σ_2 . Following the three transition points, we divide the interval $(0, \sigma_2)$ into four subintervals, i.e., $(0, \sigma_{2,0})$, $(\sigma_{2,0}, \sigma_{2,1})$, $(\sigma_{2,1}, \sigma_{2,2})$, and $(\sigma_{2,2}, \sigma_2)$. The behavior of the dispersion curves is similar in each subinterval and changes when σ passes through a transition point. As shown in Fig. 2(b), for $\sigma = 4 < \sigma_{2,0}$, there are two and six EPs located on the dispersion curves of RGMs and RIMs, respectively. For convenience, we show the values of k_0 and β of these EPs for varying σ in Fig. 3. It can be seen that EPs 5–8 tend to infinity as $\sigma \rightarrow 0$. This is because the dispersion curves of RGMs and RIMs extend to infinity

as $\sigma \rightarrow 0$. As σ is increased to $\sigma_{2,0}$, EPs 4 and 5 merge to a point marked by a magenta upward triangle in Figs. 2(c) and 3. The magenta triangle corresponds to a third-order EP where $d^2 k_0/d\beta^2 = dk_0/d\beta = 0$. For $\sigma = 5.5 > \sigma_{2,0}$, as shown in Fig. 2(d), these two EPs disappear.

As σ is increased to $\sigma_{2,1}$, from Figs. 2(e) and 3, it is observed that EPs 3 and 7 approach to a point (marked by a red asterisk) on the lightline. The transition point $\sigma_{2,1}$ has been studied in Ref. [38]. It corresponds to the case where the second dispersion curve of RGMs is not tangential to the lightline at one cutoff point. The point where EPs 3 and 7 coalesce is exactly the cutoff point with $k_c h \approx 2.3392$. From Fig. 2(e), we observe that the dispersion curve of RIMs is also not tangential to the lightline at this cutoff point. For $\sigma = 6.2 > \sigma_{2,1}$, as shown in Figs. 2(f) and 3, EPs 3 and 7 disappear but two new EPs, 9 and 10, emerge.

As σ is further increased to $\sigma_{2,2}$, from Figs. 2(g) and 3, we can see that EPs 8 and 9 merge at a point marked by a blue downward triangle. The blue triangle corresponds to a third-order EP where $d^2 \beta/dk_0^2 = d\beta/dk_0 = 0$. This phenomenon has been observed and discussed in our previous work [38]. For $\sigma > \sigma_{2,2}$, it can be seen that EPs 8 and 9 disappear and there are only four EPs remaining in Figs. 2(h) and 3. These four EPs can survive until $\sigma = \sigma_2$. We show the dispersion curves for $\sigma = \sigma_2$ in Fig. 2(i). The dispersion curve of RGMs degenerates to a point (marked by a blue hexagram) on the lightline. For $\sigma > \sigma_2$, the dispersion curve of RIMs detach from the lightline.

As shown in Fig. 3, exceptional lines formed by EPs can show different asymptotic behavior near third-order EPs, i.e., a cusp singularity or a smooth parabola [47,48]. The asymptotic behavior should depend on the properties of the EPs. For example, EPs 4 and 5 are k_0 -EPs and they merge at a cusp singularity in the σ - k_0 plane but a smooth parabola in the σ - β plane. The case for the coalescence of EPs 8 and 9 is the opposite.

IV. THE CONNECTION BETWEEN THE DISPERSION CURVES OF DIFFERENT EIGENMODES

For a lossless slab waveguide, it is known that the dispersion curves of leaky and resonant modes are connected to the dispersion curves of RIMs at k_0 -EPs and β -EPs, respectively [46]. In this section, we study the connection between dispersion curves of different eigenmodes in \mathcal{PT} -symmetric slab waveguides. We consider complex dispersion curves connected to the second dispersion curves of RGMs and RIMs. The case for $l \neq 2$ is similar. The dispersion curves of various eigenmodes for $\sigma = 4$ are shown in Fig. 4. It can be seen that there are eight EPs (numbered 1 to 8) on the dispersion curves of RGMs and RIMs. The leaky and resonant modes are connected with the RIMs at EPs 2, 4, 5 (k_0 -EP) and EPs 1, 3, 6 (β -EP), respectively. The CPGMs and CFGMs are connected with the RGMs at EP 7 (k_0 -EP) and EP 8 (β -EP), respectively. In particular, in Fig. 5, we show $\text{Im}(\beta)$ vs k_0 for eigenmodes near EPs 5 and 7, and $\text{Im}(k_0)$ vs β for eigenmodes near EPs 6 and 8. The cases for eigenmodes near EPs 1–4 are similar. In addition, for the resonant modes near EP 6, as shown in Figs. 4 and 5(b), there also exists a complex dispersion curve corresponding to the time-reversed resonant

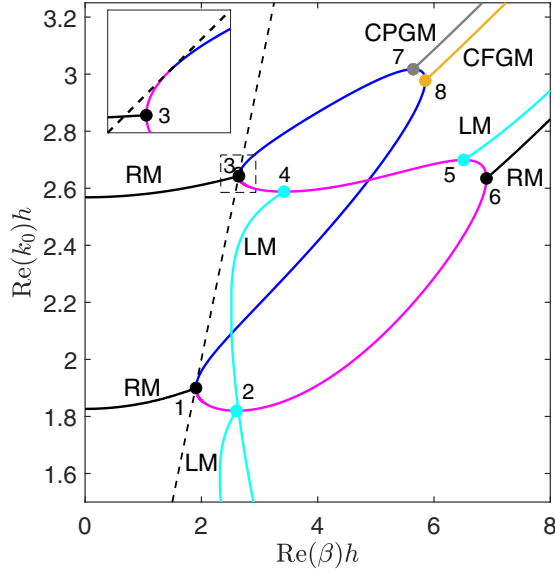


FIG. 4. The dispersion curves for $\sigma = 4$. The dashed black line is the lightline. Orange, gray, cyan, and black solid lines represent CFGMs, CPGMs, leaky modes (LM), and resonant modes (RM), respectively.

modes with $\text{Im}(k_0) > 0$. The case for the leaky modes near EP 5 is similar.

Figures 4 and 5 are results for a single σ ($\sigma = 4$). It is generally true that for all $\sigma < \sigma_l$, the complex dispersion curves of improper modes are connected to the dispersion curves of RIMs, and the dispersion curves of CPGMs and CFGMs are connected with the dispersion curves of RGMs at k_0 -EPs and β -EPs, respectively. As we have discussed in

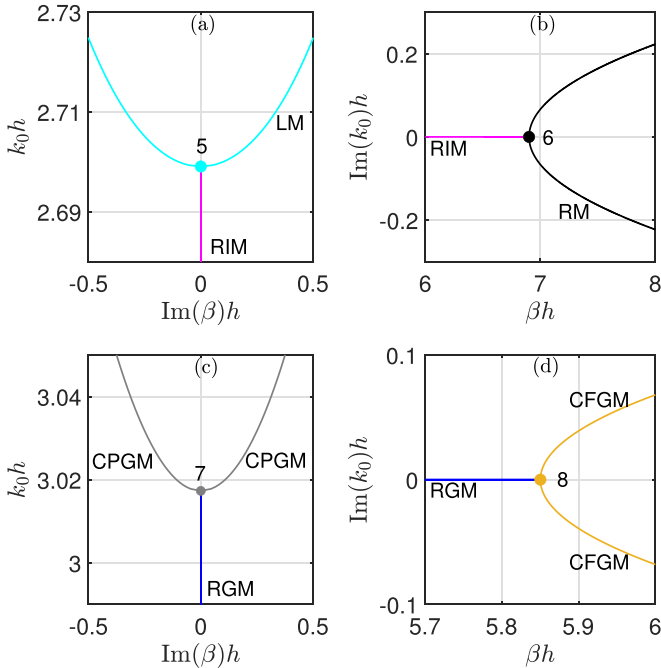


FIG. 5. The dispersion curves near EPs for $\sigma = 4$. (a) EP 5, (b) EP 6, (c) EP 7, and (d) EP 8.

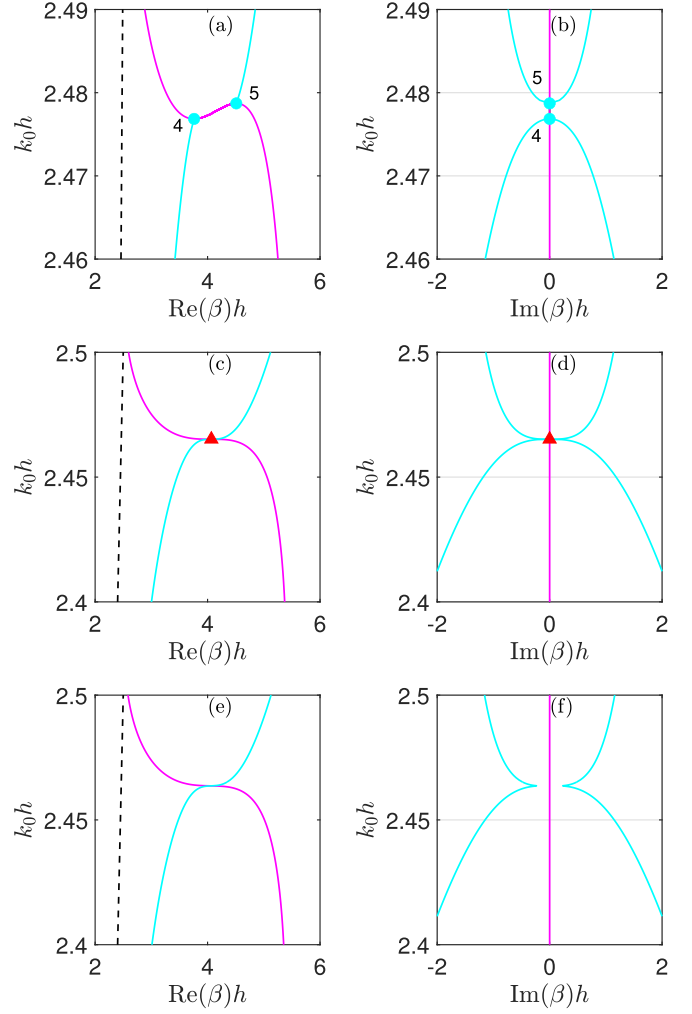


FIG. 6. The dispersion curves for various values of σ . (a) and (b) $\sigma = 5$; (c) and (d) $\sigma = \sigma_{2,0}$; (e) and (f) $\sigma = 5.09$.

Sec. III, an EP may disappear or emerge when σ passes through a transition point. In the following, we analyze the connection between the dispersion curves for σ around the transition points. First, we consider the transition point $\sigma_{2,0}$ where EP 4 and EP 5 coalesce to a third-order EP on the dispersion curve of RIMs. We show the dispersion curves of RIMs, leaky modes, and their time reversal for $\sigma = 5$, $\sigma_{2,0}$, and 5.09 in Fig. 6. For $\sigma = 5 < \sigma_{2,0}$, it can be seen that the complex dispersion curves emerging from EP 4 and EP 5 are separated from each other. For $\sigma = \sigma_{2,0}$, these dispersion curves pass through the third-order EP. For $\sigma = 5.09 > \sigma_{2,0}$, as shown in Fig. 6(f), the complex dispersion curves detach from the RIMs since the two EPs have disappeared.

Next, we consider the transition point $\sigma_{2,1}$ where the dispersion curve of RGMs and RIMs are not tangential to the lightline at a cutoff point (originated from EP 3 and EP 7). In Fig. 7, we show the dispersion curves of RGMs, RIMs, and various complex eigenmodes connected to EPs 9 and 10, and the cutoff point (marked by a red asterisk), for $\sigma = \sigma_{2,1}$ and 6.2. From Fig. 7(a), we can see that two dispersion curves (for resonant modes and CPGMs, respectively) emerge from the cutoff point on the lightline. For

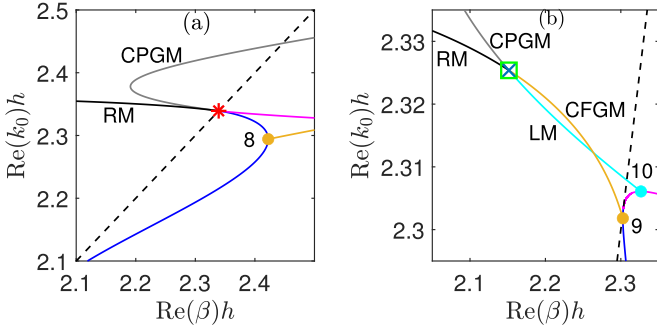


FIG. 7. The dispersion curves for $\sigma = \sigma_{2,1}$ [(a)] and $\sigma = 6.2$ [(b)]. The green square and gray blue cross represent a pair of lasing-threshold and perfect-absorption modes.

$\sigma = 6.2 > \sigma_{2,1}$, as shown in Fig. 7(b), the behavior of the dispersion curves is quite different. Two new EPs, (9 and 10), emerged on the dispersion curves of RGMs and RIMs, respectively. Connected to EPs 9 and 10, there are two dispersion curves for CFGMs and leaky modes, respectively. As shown in Figs. 7(b) and 8(a), when β is further decreased, CFGMs are transformed to resonant modes and their time reversal. The transition occurs at $\beta = \beta_* \approx 2.1516/h$ and $k_0 = k_{0,*} \approx 2.3254/h$ (both β_* and $k_{0,*}$ are real), and the corresponding eigenmodes are a lasing-threshold mode and a perfect-absorption mode. As shown in Figs. 7(b) and 8(b), when k_0 is further increased, leaky modes and their time reversal are transformed to CPGMs at the same transition point (β_* and $k_{0,*}$).

In fact, the lasing-threshold and perfect-absorption modes emerge from the cutoff point on the lightline for $\sigma > \sigma_{2,1}$. In Fig. 9, we show the dependence of EPs (3, 7, 9, and 10), the lasing-threshold mode, and the perfect-absorption mode on σ . We emphasize that the lasing-threshold and perfect-absorption modes are obtained at the connection point between the proper and improper modes, and their fields are bounded at infinity.

Finally, we consider the transition point $\sigma_{2,2}$ where EPs 8 and 9 coalesce to a third-order EP on the dispersion curve of RGMs. We show the dispersion curves of RGMs, RIMs, and CFGMs for $\sigma = \sigma_{2,2}$ and 6.3 in Fig. 10. For $\sigma = \sigma_{2,2}$, as shown in Figs. 10(a) and 10(c), the dispersion curves of CFGMs pass through the third-order EP. For $\sigma = 6.3 > \sigma_{2,2}$,

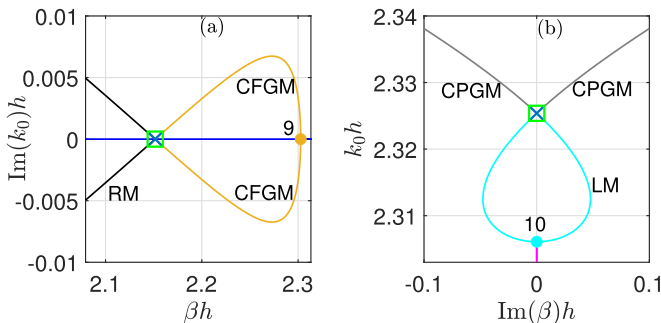


FIG. 8. The dispersion curves emerging from EP 9 and EP 10 for $\sigma = 6.2$.

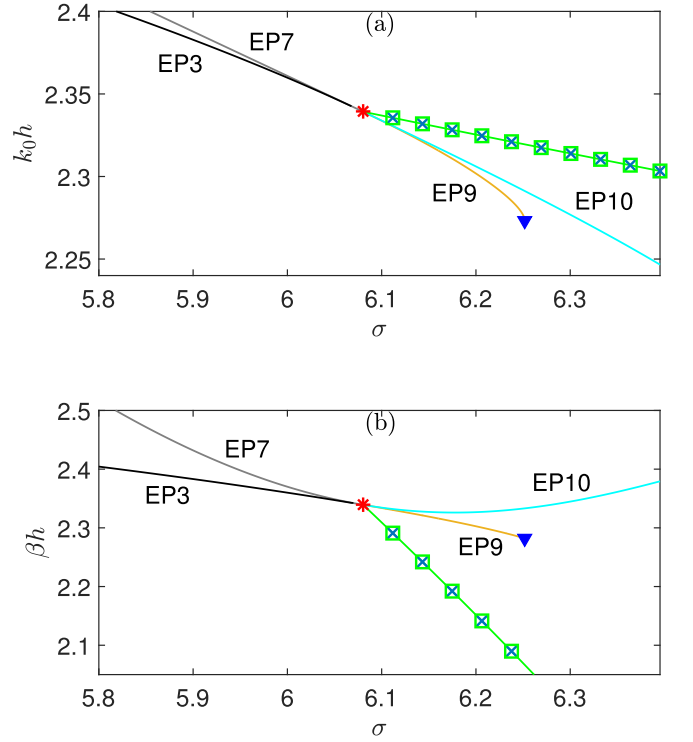


FIG. 9. The free-space wave number k_0 and the propagation constant β of EPs for varying σ . A pair of lasing-threshold (gray blue cross) and perfect-absorption modes (green square) emerge for $\sigma > \sigma_{2,1}$.

as shown in Figs. 10(b) and 10(d), the dispersion curves of CFGMs detach from the RGMs since the two EPs have disappeared.

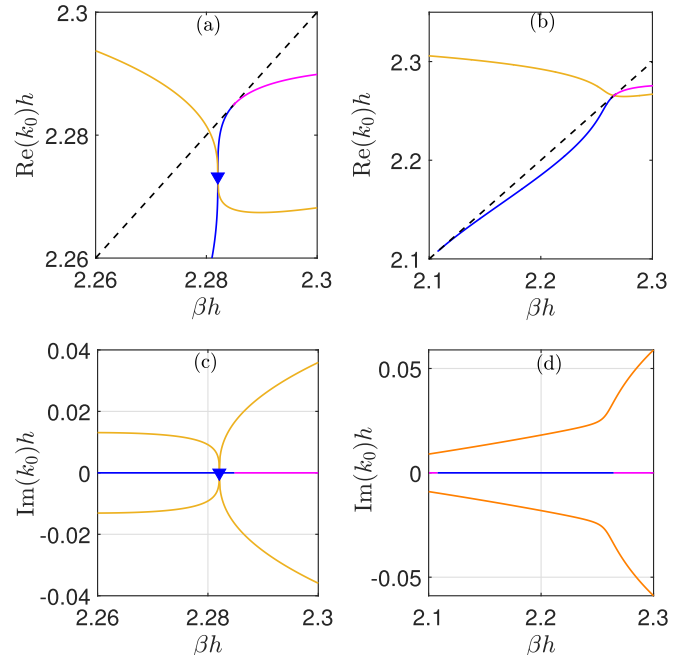


FIG. 10. The dispersion curves for $\sigma = \sigma_{2,2}$ [(a) and (c)], and $\sigma = 6.3$ [(b) and (d)].

V. SUMMARY

In this paper, we analyzed various eigenmodes in a \mathcal{PT} -symmetric slab waveguide. Most existing works on \mathcal{PT} -symmetric waveguides are concerned with various guided modes. We studied the dispersion curves of various eigenmodes and focus on the connection between the real and complex dispersion curves. It is shown that the complex dispersion curves of improper modes are connected with the dispersion curves of RIMs at EPs. The dispersion curves of CPGMs and CFGMs are connected with the dispersion curves of RGMs at the k_0 -EPs and the β -EPs, respectively. As σ is varied, there exist transition points on the dispersion curves of RGMs and RIMs. One transition point corresponds to the case where the dispersion curves of RGMs and RIMs are not tangential to the lightline at one cutoff point. Moreover, it

was shown that this cutoff point is also the limiting point of lasing-threshold and perfect-absorption modes. Our study reveals the complexity of various eigenmodes with complex ω or β , and the existence of lasing-threshold and perfect-absorption modes. Although the structure considered in this paper is a simple \mathcal{PT} -symmetric slab waveguide, we believe that the wave phenomena revealed in this paper can be found in other \mathcal{PT} -symmetric waveguides.

ACKNOWLEDGMENTS

The authors acknowledge support from the Research Grants Council of Hong Kong Special Administrative Region, China (Grant No. CityU 11305021).

- [1] C. M. Bender and S. Boettcher, Real spectra in non-Hermitian Hamiltonians having \mathcal{PT} symmetry, *Phys. Rev. Lett.* **80**, 5243 (1998).
- [2] C. M. Bender, S. Boettcher, and P. N. Meisinger, \mathcal{PT} -symmetric quantum mechanics, *J. Math. Phys.* **40**, 2201 (1999).
- [3] C. M. Bender, D. C. Brody, and H. F. Jones, Complex extension of quantum mechanics, *Phys. Rev. Lett.* **89**, 270401 (2002).
- [4] H.-P. Nolting, G. Sztefka, M. Grawert, and J. Ctyroky, Wave propagation in a waveguide with a balance of gain and loss, in *Integrated Photonics Research* (Optica Publishing Group, Washington, DC, 1996), pp. 76–79.
- [5] R. El-Ganainy, K. G. Makris, D. N. Christodoulides, and Z. H. Musslimani, Theory of coupled optical \mathcal{PT} -symmetric structures, *Opt. Lett.* **32**, 2632 (2007).
- [6] S. Klaiman, U. Günther, and N. Moiseyev, Visualization of branch points in \mathcal{PT} -symmetric waveguides, *Phys. Rev. Lett.* **101**, 080402 (2008).
- [7] K. G. Makris, R. El-Ganainy, D. N. Christodoulides, and Z. H. Musslimani, Beam dynamics in \mathcal{PT} symmetric optical lattices, *Phys. Rev. Lett.* **100**, 103904 (2008).
- [8] A. Guo, G. J. Salamo, D. Duchesne, R. Morandotti, M. Volatier-Ravat, V. Aimez, G. A. Siviloglou, and D. N. Christodoulides, Observation of \mathcal{PT} -symmetry breaking in complex optical potentials, *Phys. Rev. Lett.* **103**, 093902 (2009).
- [9] A. Mostafazadeh, Spectral singularities of complex scattering potentials and infinite reflection and transmission coefficients at real energies, *Phys. Rev. Lett.* **102**, 220402 (2009).
- [10] C. E. Rüter, K. G. Makris, R. El-Ganainy, D. N. Christodoulides, M. Segev, and D. Kip, Observation of parity-time symmetry in optics, *Nat. Phys.* **6**, 192 (2010).
- [11] A. A. Zyblovsky, A. P. Vinogradov, A. A. Pukhov, A. V. Dorofeenko, and A. A. Lisiansky, \mathcal{PT} -symmetry in optics, *Phys.-Usp.* **57**, 1063 (2014).
- [12] L. Feng, R. El-Ganainy, and L. Ge, Non-Hermitian photonics based on parity-time symmetry, *Nat. Photon.* **11**, 752 (2017).
- [13] R. El-Ganainy, K. G. Makris, M. Khajavikhan, Z. H. Musslimani, S. Rotter, and D. N. Christodoulides, Non-Hermitian physics and \mathcal{PT} symmetry, *Nat. Phys.* **14**, 11 (2018).
- [14] S. Longhi, Parity-time symmetry meets photonics: A new twist in non-Hermitian optics, *Europhys. Lett.* **120**, 64001 (2017).
- [15] Ş. K. Özdemir, S. Rotter, F. Nori, and L. Yang, Parity–time symmetry and exceptional points in photonics, *Nat. Mater.* **18**, 783 (2019).
- [16] Z. Lin, H. Ramezani, T. Eichelkraut, T. Kottos, H. Cao, and D. N. Christodoulides, Unidirectional invisibility induced by \mathcal{PT} -symmetric periodic structures, *Phys. Rev. Lett.* **106**, 213901 (2011).
- [17] S. Longhi, Invisibility in \mathcal{PT} -symmetric complex crystals, *J. Phys. A: Math. Theor.* **44**, 485302 (2011).
- [18] Y. Huang, Y. Shen, C. Min, S. Fan, and G. Veronis, Unidirectional reflectionless light propagation at exceptional points, *Nanophotonics* **6**, 977 (2017).
- [19] L. Yuan and Y. Y. Lu, Unidirectional reflectionless transmission for two-dimensional \mathcal{PT} -symmetric periodic structures, *Phys. Rev. A* **100**, 053805 (2019).
- [20] S. Longhi, Bloch oscillations in complex crystals with \mathcal{PT} symmetry, *Phys. Rev. Lett.* **103**, 123601 (2009).
- [21] M. A. Miri, P. Likamwa, and D. N. Christodoulides, Large area single-mode parity-time-symmetric laser amplifiers, *Opt. Lett.* **37**, 764 (2012).
- [22] W. Liu, L. Ming, R. S. Guzzon, E. J. Norberg, and J. Yao, An integrated parity-time symmetric wavelength-tunable single-mode microring laser, *Nat. Commun.* **8**, 15389 (2017).
- [23] S. Longhi, \mathcal{PT} -symmetric laser absorber, *Phys. Rev. A* **82**, 031801(R) (2010).
- [24] Y. D. Chong, L. Ge, and A. D. Stone, \mathcal{PT} -symmetry breaking and laser-absorber modes in optical scattering systems, *Phys. Rev. Lett.* **106**, 093902 (2011).
- [25] Y. Sun, W. Tan, H.-Q. Li, J. Li, and H. Chen, Experimental demonstration of a coherent perfect absorber with \mathcal{PT} phase transition, *Phys. Rev. Lett.* **112**, 143903 (2014).
- [26] J. Čtyroký, V. Kuzmiak, and S. Eyderman, Waveguide structures with antisymmetric gain/loss profile, *Opt. Express* **18**, 21585 (2010).
- [27] J. Čtyroký, Dispersion properties of coupled waveguides with loss and gain: a full-vectorial analysis, *Opt. Quant. Electron.* **46**, 465 (2014).
- [28] C. Huang, F. Ye, and X. Chen, Mode pairs in \mathcal{PT} -symmetric multimode waveguides, *Phys. Rev. A* **90**, 043833 (2014).

- [29] N. X. A. Rivolta and B. Maes, Symmetry recovery for coupled photonic modes with transversal PT symmetry, *Opt. Lett.* **40**, 3922 (2015).
- [30] H. Benisty, A. Lupu, and A. Degiron, Transverse periodic \mathcal{PT} symmetry for modal demultiplexing in optical waveguides, *Phys. Rev. A* **91**, 053825 (2015).
- [31] H. Alaeian, B. Baum, V. Jankovic, M. Lawrence, and J. A. Dionne, Towards nanoscale multiplexing with parity-time-symmetric plasmonic coaxial waveguides, *Phys. Rev. B* **93**, 205439 (2016).
- [32] N. Moiseyev and M. Šindelka, Transfer of information through waveguides near an exceptional point, *Phys. Rev. A* **103**, 033518 (2021).
- [33] H. Alaeian and J. A. Dionne, Non-Hermitian nanophotonic and plasmonic waveguides, *Phys. Rev. B* **89**, 075136 (2014).
- [34] S. Savoia, G. Castaldi, and V. Galdi, Non-Hermiticity-induced wave confinement and guiding in loss-gain-loss three-layer systems, *Phys. Rev. A* **94**, 043838 (2016).
- [35] T. Goldzak, A. A. Mailybaev, and N. Moiseyev, Light stops at exceptional points, *Phys. Rev. Lett.* **120**, 013901 (2018).
- [36] L. Zhang, L. Ying, L. Ge, W. Zhao, and W. Zhang, Extraordinary fast forward and backward light in transparent non-Hermitian systems, *Laser Photonics Rev.* **15**, 2000204 (2021).
- [37] X.-Z. Zhang, R.-Z. Luo, and J. Chen, Revisit the Poynting vector in \mathcal{PT} -symmetric coupled waveguides, *Opt. Express* **30**, 38753 (2022).
- [38] N. Zhang and Y. Y. Lu, Guided modes in a \mathcal{PT} -symmetric waveguide: Real dispersion curves, *Phys. Rev. A* **108**, 053508 (2023).
- [39] S. Yamaguchi, A. Shimojima, and T. Hosono, Analysis of leaky modes supported by a slab waveguide, *Electron. Commun. Jpn. Pt. II* **73**, 20 (1990).
- [40] J. Hu and C. R. Menyuk, Understanding leaky modes: slab waveguide revisited, *Adv. Opt. Photonics* **1**, 58 (2009).
- [41] S. Savoia, G. Castaldi, V. Galdi, A. Alù, and N. Engheta, \mathcal{PT} -symmetry-induced wave confinement and guiding in ε -near-zero metamaterials, *Phys. Rev. B* **91**, 115114 (2015).
- [42] M. Hajizadegan, L. Zhu, and P.-Y. Chen, Superdirective leaky radiation from a PT -synthetic metachannel, *Opt. Express* **29**, 12330 (2021).
- [43] S. Fan and J. D. Joannopoulos, Analysis of guided resonances in photonic crystal slabs, *Phys. Rev. B* **65**, 235112 (2002).
- [44] Q. Song, J. Hu, S. Dai, C. Zheng, D. Han, J. Zi, Z. Q. Zhang, and C. T. Chan, Coexistence of a new type of bound state in the continuum and a lasing threshold mode induced by PT symmetry, *Sci. Adv.* **6**, eabc1160 (2020).
- [45] G. W. Hanson and A. B. Yakovlev, An analysis of leaky-wave dispersion phenomena in the vicinity of cutoff using complex frequency plane singularities, *Radio Sci.* **33**, 803 (1998).
- [46] A. Abdrabou and Y. Y. Lu, Indirect link between resonant and guided modes on uniform and periodic slabs, *Phys. Rev. A* **99**, 063818 (2019).
- [47] K. Ding, C. Fang, and G. Ma, Non-Hermitian topology and exceptional-point geometries, *Nat. Rev. Phys.* **4**, 745 (2022).
- [48] R.-Y. Zhang, X. Cui, W.-J. Chen, Z.-Q. Zhang, and C. T. Chan, Symmetry-protected topological exceptional chains in non-Hermitian crystals, *Commun. Phys.* **6**, 169 (2023).